Energy Conservation and Convergence of High-Order Mimetic Schemes for the 3D Advection Equation

Miguel A. Dumett and Jose E. Castillo

July 21, 2023

Publication Number: CSRCR2023-05

Computational Science & Engineering Faculty and Students Research Articles

Database Powered by the Computational Science Research Center Computing Group & Visualization Lab

COMPUTATIONAL SCIENCE & ENGINEERING

SAN DIEGO STATE UNIVERSITY

Computational Science Research Center
College of Sciences
5500 Campanile Drive
San Diego, CA 92182-1245
(619) 594-3430

Energy Conservation and Convergence of High-Order Mimetic Schemes for the 3D Advection Equation *

Miguel A. Dumett † Jose E. Castillo ‡

July 21, 2023

Abstract

In this paper, it is demonstrated theoretically that high-order mimetic discrete analogs (for the spatial derivatives) of the three-dimensional advection equation conserves energy, if an energy preserving time discretization scheme is utilized. In addition, it is proposed a mimetic scheme that uses the fourth-order Corbino-Castillo mimetic discrete analog of the advection equation together with the sixth-order filtered leapfrog method LF-MMK time discretization scheme [9] that conserves total energy. It is proved that this algorithm converges numerically. The LF-MMK scheme is an ordinary differential equation method that introduces three additional stage variables to the discrete mimetic space variable, for which there is no dynamical system. Before the converge proof is given, an ordinary differential system is found for all four variables.

1 Introduction

In [5], it is demonstrated that one-dimensional (1D) second-order mimetic discrete analog of the 1D advection equation conserves energy. That is a property that any mimetic difference method holds provided that the method satisfies a discrete analog of the integration by parts formula [1, 2, 3].

This work not only generalizes to the three-dimensional (3D) advection equation the energy conservation of mimetic discrete analogs of the one-dimensional (1D) advection equation in [5] but also proposes a uses a fourth-order mimetic scheme in space and and a sixth-order filtered leapfrog method for simulating the 3D advection equation, for which a convergence proof is given.

*This work was partially supported by SDSU

†Computational Science Research Center at the San Diego State University (mdumett@sdsu.edu).

‡Computational Science Research Center at the San Diego State University (jcastillo@sdsu.edu).

In particular, the stability part of the convergence argument relies on the properties of the eigenvalues of the divergence and gradient mimetic operators (for which the Corbino-Castillo operators [3] are utilized but it can be demonstrated that similar properties hold for the Castillo-Grone method [1, 2]), when combined with the corresponding high-order mimetic interpolation operators.

The time-discretization part of the designed algorithm is a method-of-lines type scheme for the mimetic analog of the 3D advection equation of the spatial derivatives, that utilizes four-stage discrete vector variables (one that contains the spatial variations from the mimetic analog) and the other three from the time discretization method itself.

Consistency and stability discussions require an ordinary differential equation (ODE) for each of the four discrete vector variables involved in the time-discretization scheme. Only one ODE is available (for the discrete vector variable that comes from the mimetic discrete analog part of the spatial derivatives of the equation). This document proposes a way of deriving such ODEs for each of the other three discrete vector variables. Once this is established, the consistency (order of accuracy) and stability properties of the mimetic scheme are determined.

In Section 2, the 3D advection equation in $\mathbb{R}^3$ is introduced.

Section 3 begins with the 3D advection equation on $[-1, 1]^3$ with boundary conditions. Then the mimetic integral form of the equations is obtained and the staggered grid utilized is presented. Then, the discrete energy and some mimetic operator are evoked. The section finished with a proof that high-order mimetic difference discrete analog of the 3D advection equation has the property of energy conservation.

Section 4 demonstrates the convergence of a high-order mimetic scheme for the 3D advection equation. Section 4 initially focuses on the mimetic analog of the flux part of the 3D advection equation. Then, it introduces the sixth-order filtered leapfrog scheme LF-MMK, a method-of-lines type [9] and hooks it up with the mimetic analog of the 3D advection flux. Furthermore, in this section, an appropriate ODE system is found for all the four-stage variables of the LF-MMK scheme before starting the convergence study of the mimetic scheme proposed. The stability part of the proof relies on the eigenvalues of the mimetic divergence and gradient operators when clumped together with their respective high-order mimetic interpolation operators [6] (see Appendix A).

The tensor nature of the high-order 3D mimetic operators (which are defined by Kronecker products) causes that the numerical simulation of the 1D advection equation in Section 5, are enough for demonstrating that the high-order mimetic scheme works. Time evolution and energy conservation plots are also shown in Section 5.

In Section 6, some conclusions are drawn.

2 The 3D advection equation

Consider the following 3D advection partial differential equation (without boundary conditions) on $V = \mathbb{R}^3$, with known constant velocity $v = (v_1, v_2, v_3)^t$, for the unknown scalar field $u = u(x, y, z)$,

$$\begin{aligned} u_t(x,y,z,t) + \nabla \cdot (u\vec{v}) &= 0, \qquad x \in V, \quad t > 0, && (1)\\ u(x,y,z,0) &= u_0(x,y,z), \qquad (x,y,z) \in V, && (2) \end{aligned}$$

where u_0 is a smooth enough function. It is well-known that (1)-(2) is a well-posed PDE. The initial data propagates following the constant velocity vector v [7, p.18].

3 Energy conservation of mimetic differences

In this section, it is proven that, for the advection equation with smooth initial and boundary data, a high-order mimetic difference scheme, when combined with a leapfrog method and a sixth-order time filter, conserves energy.

3.1 The 3D advection PDE with boundary conditions

Consider the following 3D advection partial differential equation (or, linear transport equation) on $V = [-1, 1]^3$, with known constant velocity $v = (v_1, v_2, v_3)^t$, for the unknown scalar field $u = u(x, y, z)$,

$$\begin{aligned} u_t(x,y,z,t) + \nabla \cdot (uv) &= 0, \qquad (x,y,z) \in V, \quad t > 0, && (3)\\ u(-1,y,z,t) &= g_1(y,z,t), \ (x,y,z) \in \{-1\} \times (-1,1) \times (-1,1), \ t > 0, && (4)\\ u(x,-1,z,t) &= g_2(x,z,t), \ (x,y,z) \in (-1,1) \times \{-1\} \times (-1,1), \ t > 0, && (5)\\ u(x,y,-1,t) &= g_3(x,y,t), \ (x,y,z) \in (-1,1) \times (-1,1) \times \{-1\}, \ t > 0, && (6)\\ u(x,y,z,0) &= u_0(x,y,z), && (7) \end{aligned}$$

where g_1, g_2, g_3, u_0, are smooth enough functions, such there is enough differentiability among their values on the common boundaries.

3.1.1 The integral problem

By multiplying (3) by u and integrating over the spatial domain, one obtains

$$\int_V u\, u_t \, dV + \int_V u \, \nabla \cdot (u\vec{v}) \, dV = 0, \tag{8}$$

with dV the Cartesian volume element.

The first and second terms in (8) verify

$$\begin{aligned}\int_V u\, u_t\, dV &= \int_V \frac{1}{2}\frac{du^2}{dt}\, dV = \frac{1}{2}\frac{d}{dt}\left(\int_V u^2\, dV\right),\\ \int_V u\, \nabla\cdot(\vec{v}\cdot u)\, dV &= \frac{1}{2}\int_V \nabla\cdot(u^2\vec{v})\, dV,\end{aligned}$$

and hence, after a time integration from 0 to T, (8) becomes

$$\int_V (u^2(x,y,z,T) - u^2(x,y,z,0))\, dx + \int_0^T \int_V \nabla\cdot(u^2\vec{v})\, dV\, dt = 0. \tag{9}$$

3.2 The mimetic discrete analog of the integral problem

Before establishing the energy conservation of the mimetic discrete analog of the integral equation, some mimetic preliminaries are given.

3.2.1 The staggered grid

Let m, n, o are the number of cells along the $x-, y-, z-$axes, respectively. On the axes-uniform staggered grid $S = S_m \times S_n \times S_o$, where

$$S_p = \{-1 = s_0, s_{\frac{1}{2}}, \cdots, s_{p-\frac{1}{2}}, s_{p+1} = 1\},$$

with $s_{j-\frac{1}{2}} = -1 + (j - \frac{1}{2})h_p$, $h_p = \frac{2}{p}$, $j = 1, \cdots, p$, define $U(s_i, s_j, s_l, t)$, the mimetic numerical approximation of $u(x_i, y_j, z_l, t)$, at time coordinate t and space coordinates $s_i = x_i, s_j = y_j, s_l = z_l$.

In addition, define $U(t) = U(S_m, S_n, S_o, t)$, the numerical approximation on grid S at time t, and the discrete element volume $h = h_m h_n h_o$. Notice that $U(0) = u_0$.

For the approximation of the vector field, it is convenient to define the grid

$$N = (S_m \times N_n \times N_o) \cup (N_m \times S_n \times N_o) \cup (N_m \times N_n \times S_o),$$

the middle edges of the voxels with centers at $S_m^0 \times S_n^0 \times S_o^0$, where

$$N_q = \{r_1, \cdots, r_{q-1}\},$$

with $r_j = -1 + j\, h_q$, $h_q = \frac{2}{q}$, $j = 1, \cdots, q-1$, and $S_p^0 = S_p \setminus \{s_0, s_{p+1}\}$.

In mimetic differences, approximation U of scalar field u are defined on $S_m \times S_n \times S_o$, while approximation $\mathcal{V}$ of vector fields v are defined on $N_m \times N_n \times N_o$.

3.2.2 The discrete energy term

Since there are no divergence or gradient operators in the volume integral $\int_V u^2\, dV$ at time t, it is approximated by

$$h\,(\mathrm{vec}_L(U(t)))^T \mathrm{vec}_L(U(t)),$$

vec_L is the vectorization operator of the three-dimensional tensor $U(t)$, that maps the discrete $U(t)$-cube onto a vector of length $d = (m+2)(n+2)(o+2)$, following the lexicographic ordering.

Observe that for the scalar field, $\int_V u^2(x,y,z,t)\, dV$ is called the energy at time t, and one can define the discrete energy E_d of $U(t)$ at time t by

$$E_d(t) = h\,(\mathrm{vec}_L(U(t)))^T \mathrm{vec}_L(U(t)).$$

3.2.3 Some mimetic operators in 3D

The 3D of order k, $k = 2, 4, 6, 8$, divergence interpolation operator that maps S onto N is

$$\mathcal{I}_D^k = \begin{bmatrix} \hat{I}_o^T \otimes \hat{I}_n^T \otimes I_{D_x}^k & & \\ & \hat{I}_o^T \otimes I_{D_y}^k \otimes \hat{I}_m^T & \\ & & I_{D_z}^k \otimes \hat{I}_n^T \otimes \hat{I}_m^T \end{bmatrix},$$

with $I_{D_r}^k$, $r = x, y, z$, the 1D interpolation operator on the r-axis [4], and

$$\hat{I}_p = \begin{bmatrix} 0 & \cdots & \\ 1 & & \\ & \ddots & \\ & & 1 \\ & \cdots & 0 \end{bmatrix},$$

the extension of the identity matrix by adding two extra rows of zeros (one at the top and one at the bottom). Notice that the $\mathcal{I}_D^k \in \mathbb{R}^{b\times c}$, where

$$b = (m+1)no + m(n+1)o + mn(o+1),$$

is the cardinality of mimetic discrete vector fields in 3D, and

$$c = (m+2)(n+2)(o+2)$$

is the cardinality of mimetic discrete scalar fields in 3D.

The weight matrix for the d-dimensional divergence operator is

$$\mathcal{Q}^k = \begin{bmatrix} I_{o+2} \otimes I_{n+2} \otimes Q_{m+2}^k & & \\ & I_{o+2} \otimes Q_{n+2}^k \otimes I_{m+2} & \\ & & Q_{o+2}^k \otimes I_{n+2} \otimes I_{m+2} \end{bmatrix},$$

where Q_p^k is the $p \times p$ weight matrix for the 1D divergence operator, and I_p the $p \times p$ identity matrix.

The three-dimensional divergence operator of order k is

$$D_{xyz}^k = \left[\begin{array}{ccc} \hat{I}_o \otimes \hat{I}_n \otimes D_x^k, & \hat{I}_o \otimes D_y^k \otimes \hat{I}_m, & D_z^k \otimes \hat{I}_n \otimes \hat{I}_m \end{array} \right],$$

with D_r^k, $r = x, y, z$, the 1D divergence operator of order k on the r-axis [3].

3.3 Energy conservation of the mimetic discrete analog

In addition, since in mimetic differences of any order k, the discrete scalar field U is defined on S, needs to be interpolated, by an interpolation operator of order k, to N, to be able to approximate $\int_V 1 \nabla \cdot (u^2 \vec{v})\, dV$, without loosing accuracy.

Hence, the mimetic approximation of order k for $\int_V 1 \nabla \cdot (u^2 \vec{v})\, dV$, (see [6]) is given by

$$\langle D_{xyz}^k (\vec{\mathcal{V}} \mathcal{I}_D^k (U^2)), \mathbb{1} \rangle_{\mathcal{Q}^k} = \mathrm{vec}_L (\vec{\mathcal{V}} \mathcal{I}_D^k (U^2))^T \mathcal{Q}^k (D_{xyz}^k)^T \mathrm{vec}_L (\mathbb{1}), \tag{10}$$

where the time dependence has been omitted to simplify the notation, $\mathbb{1}$ is the constant one discrete scalar field on S, and $\vec{\mathcal{V}}$ is the discrete version of constant vector field $\vec{v}$ [6].

In addition, in 1D one has [6]

$$h\, Q D^T \mathbb{1} = (-1, 0, \cdots, 0, 1)^T. \tag{11}$$

A direct computation of $\mathcal{Q}^k (D_{xyz}^k)^T$ gives

$$\mathcal{Q}^k D_{xyz}^T = \left[\begin{array}{c} \hat{I}_o^T \otimes \hat{I}_n^T \otimes Q_{m+2}^k {D_x^k}^T \\ \hat{I}_o^T \otimes Q_{n+2}^k {D_y^k}^T \otimes \hat{I}_m^T \\ Q_{o+2}^k {D_z^k}^T \otimes \hat{I}_n^T \otimes \hat{I}_m^T \end{array} \right]$$

and by using the properties Kronecker product and the vectorization operator, one gets

$$\begin{aligned} \mathcal{Q}^k (D_{xyz}^k)^T \mathrm{vec}_L (\mathbb{1}) &= \left[\begin{array}{c} (\hat{I}_o^T \otimes \hat{I}_n^T \otimes Q_{m+2}^k {D_x^k}^T) \mathrm{vec}_L (\mathbb{1}) \\ (\hat{I}_o^T \otimes Q_{n+2}^k {D_y^k}^T \otimes \hat{I}_m^T) \mathrm{vec}_L (\mathbb{1}) \\ (Q_{o+2}^k {D_z^k}^T \otimes \hat{I}_n^T \otimes \hat{I}_m^T) \mathrm{vec}_L (\mathbb{1}) \end{array} \right] \\ &= \left[\begin{array}{c} \mathrm{vec}_L (Q_{m+2}^k D_x^k)^T \mathbb{1}_{m+2,(n+2)(o+2)} (\hat{I}_o \otimes \hat{I}_n) \\ (\hat{I}_o^T \otimes Q_{n+2}^k {D_y^k}^T \otimes \hat{I}_m^T) \mathrm{vec}_L (\mathbb{1}) \\ (Q_{o+2}^k {D_z^k}^T \otimes \hat{I}_n^T \otimes \hat{I}_m^T) \mathrm{vec}_L (\mathbb{1}) \end{array} \right], \end{aligned} \tag{12}$$

since $(B^T \otimes A)\mathrm{vec}_L(X) = \mathrm{vec}_L(AXB^T)$, with $\mathbb{1}_{p,q}$ is a $p \times q$ matrix of ones.

From (11)

$$\begin{aligned} Q^k_{m+2} {D^k_x}^T \mathbb{1}_{m+2,(n+2)(o+2)} &= \begin{bmatrix} -1 & \cdots & -1 \\ 0 & \cdots & 0 \\ \vdots & \vdots & \vdots \\ 0 & \cdots & 0 \\ 1 & \cdots & 1 \end{bmatrix}_{(m+1)\times(n+2)(o+2)} \\ &= [-1, 0, \cdots, 0, 1]^T_{m+1} [1, \cdots, 1]_{(n+2)(o+2)}. \end{aligned} \tag{13}$$

By (13), if $M = [Q^k_{m+2} {D^k_x}^T \mathbb{1}_{m+2,(n+2)(o+2)}](\hat{I}_o \otimes \hat{I}_n)$, one obtains

$$\begin{aligned} M &= \begin{bmatrix} -1 & \cdots & -1 \\ 0 & \cdots & 0 \\ \vdots & \vdots & \vdots \\ 0 & \cdots & 0 \\ 1 & \cdots & 1 \end{bmatrix}_{(m+1)\times(n+2)(o+2)} (\hat{I}_o \otimes \hat{I}_n) \\ &= \begin{bmatrix} -1 & \cdots & -1 \\ 0 & \cdots & 0 \\ \vdots & \vdots & \vdots \\ 0 & \cdots & 0 \\ 1 & \cdots & 1 \end{bmatrix}_{(m+1),no} = [-1, 0, \cdots, 0, 1]^T_m [1, \cdots, 1]_{no}, \end{aligned} \tag{14}$$

and hence $[Q^k_{m+2} {D^k_x}^T \mathbb{1}_{m+2,(n+2)(o+2)}](\hat{I}_o \otimes \hat{I}_n)$ is the boundary information of faces $\{-1\} \times N_n \times N_o$ (with negative sign) and $\{1\} \times N_n \times N_o$ (with positive sign).

Since $A \otimes B = P_l(B \otimes A)P_r$, for some permutation matrices P_l and P_r, then the remaining rows other than the first of (12) become

$$\begin{aligned} (\hat{I}^T_o \otimes Q^k_{n+2} {D^k_y}^T \otimes \hat{I}^T_m)\mathrm{vec}_L(\mathbb{1}) &= P^{(2)}_l (\hat{I}^T_m \otimes \hat{I}^T_o \otimes Q^k_{n+2} {D^k_y}^T) P^{(2)}_r \mathrm{vec}_L(\mathbb{1}), \\ (Q^k_{o+2} {D^k_z}^T \otimes \hat{I}^T_n \otimes \hat{I}^T_m)\mathrm{vec}_L(\mathbb{1}) &= P^{(3)}_l (\hat{I}^T_n \otimes \hat{I}^T_m \otimes Q^k_{o+2} {D^k_z}^T) P^{(3)}_r \mathrm{vec}_L(\mathbb{1}), \end{aligned} \tag{15}$$

for some matrices $P^{(2)}_l, P^{(2)}_r, P^{(3)}_l, P^{(3)}_r$, respectively.

Identities (15) can also be established by induction. For 1D, (11) holds. If one assumes, it is valid for 1D and tries to proof the identity for 2D, then formulas (12)-(14) establish the

existence of $P_l^{(2)}, P_r^{(2)}$ in (15). Similarly, from the 2D identity, one can derive the existence of $P_l^{(3)}, P_r^{(3)}$ of (15).

As $\mathrm{vec}_L(\mathbb{1})$ is a vector of only ones, then $P_r^{(p)}\mathrm{vec}_L(\mathbb{1}) = \mathrm{vec}_L(\mathbb{1})$, $p = 2, 3$. Hence,

$$\begin{aligned}(\hat{I}_o^T \otimes Q_{n+2}^k D_y^{k^T} \otimes \hat{I}_m^T)\mathrm{vec}_L(\mathbb{1}) &= P_l^{(2)}\mathrm{vec}_L(Q_{n+2}^k D_y^{k^T}\mathbb{1}_{n+2,(m+2)(o+2)}(\hat{I}_m \otimes \hat{I}_o)),\\ (Q_{o+2}^k D_z^{k^T} \otimes \hat{I}_n^T \otimes \hat{I}_m^T)\mathrm{vec}_L(\mathbb{1}) &= P_l^{(3)}\mathrm{vec}_L(Q_{o+2}^k D_z^{k^T}\mathbb{1}_{o+2,(m+2)(n+2)}(\hat{I}_n \otimes \hat{I}_m)),\end{aligned} \tag{16}$$

respectively.

Similar arguments to those of (12)-(16) demonstrate that

$$\begin{aligned}Q_{n+2}^k D_y^{k^T}\mathbb{1}_{n+2,(m+2)(o+2)} &= [-1, 0, \cdots, 0, 1]_{n+1}^T[1, \cdots, 1]_{(m+2)(o+2)},\\ Q_{o+2}^k D_z^{k^T}\mathbb{1}_{o+2,(m+2)(n+2)} &= [-1, 0, \cdots, 0, 1]_{o+1}^T[1, \cdots, 1]_{(m+2)(n+2)},\end{aligned}$$

and hence, the second row of (12) is the boundary information of faces $N_m \times \{-1\} \times N_o$ (with negative sign) and $N_m\{1\} \times N_o$ (with positive sign), and the third row of (12) is the boundary information of faces $N_m \times N_n \times \{-1\}$ (with negative sign) and $N_m \times N_n \times \{1\}$ (with positive sign), respectively.

Therefore, (10) becomes

$$\begin{aligned}h\left[v_1(\mathrm{vec}_L(\mathcal{I}_D^{k^T}U^2))^T, v_2(\mathrm{vec}_L(\mathcal{I}_D^{k^T}U^2))^T, v_3(\mathrm{vec}_L(\mathcal{I}_D^{k^T}U^2))^T\right]\mathcal{Q}^k D_{xyz}^T\mathrm{vec}_L(\mathbb{1}) &=\\ h\left(v_1(\mathrm{vec}_L(\mathcal{I}_D^{k^T}U^2))^T, v_2(\mathrm{vec}_L(\mathcal{I}_D^{k^T}U^2))^T, v_3(\mathrm{vec}_L(\mathcal{I}_D^{k^T}U^2))^T\right] &\cdot\\ \begin{bmatrix}[-1, 0, \cdots, 0, 1]_{m+1}^T[1, \cdots, 1]_{(n+2)(o+2)}(\hat{I}_o \otimes \hat{I}_n)\\ P_l^{(2)}[-1, 0, \cdots, 0, 1]_{n+1}^T[1, \cdots, 1]_{(m+2)(o+2)}(\hat{I}_m \otimes \hat{I}_o)\\ P_l^{(3)}[-1, 0, \cdots, 0, 1]_{o+1}^T[1, \cdots, 1]_{(m+2)(n+2)}(\hat{I}_n \otimes \hat{I}_m)\end{bmatrix} &=\\ h[v_1(\mathrm{vec}_L(\mathcal{I}_D^{k^T}U^2))^T[-1, 0, \cdots, 0, 1]_{m+1}^T[1, \cdots, 1]_{(n+2)(o+2)}(\hat{I}_o \otimes \hat{I}_n) &+\\ v_2(\mathrm{vec}_L(\mathcal{I}_D^{k^T}U^2))^T P_l^{(2)}[-1, 0, \cdots, 0, 1]_{n+1}^T[1, \cdots, 1]_{(m+2)(o+2)}(\hat{I}_m \otimes \hat{I}_o) &+\\ v_3(\mathrm{vec}_L(\mathcal{I}_D^{k^T}U^2))^T P_l^{(3)}[-1, 0, \cdots, 0, 1]_{o+1}^T[1, \cdots, 1]_{(m+2)(n+2)}(\hat{I}_n \otimes \hat{I}_m)] &=\end{aligned}$$

$$\begin{aligned}h\Bigg[v_1\sum_{j=1}^{n-1}\sum_{l=1}^{o-1}(U^2(1, r_j, r_l, t) - U^2(-1, r_j, r_l, t)) + v_2\sum_{i=1}^{m-1}\sum_{l=1}^{o-1}(U^2(r_i, 1, r_l, t) - U^2(r_i, -1, r_l, t)) &+\\ v_3\sum_{i=1}^{m-1}\sum_{j=1}^{n-1}(U^2(r_i, r_j, 1, t) - U^2(r_i, r_j, -1, t))\Bigg].&\end{aligned}$$

Therefore, the mimetic discrete analog of (9) is given by

$$E_d(T) + h\left[v_1\sum_{j=1}^{n-1}\sum_{l=1}^{o-1}U^2(1,r_j,r_l,t) + v_2\sum_{i=1}^{m-1}\sum_{l=1}^{o-1}U^2(r_i,1,r_l,t) + v_3\sum_{i=1}^{m-1}\sum_{j=1}^{n-1}U^2(r_i,r_j,1,t)\right] =$$
$$E_d(0) + h\left[v_1\sum_{j=1}^{n-1}\sum_{l=1}^{o-1}g_1^2(r_j,r_l,t) + v_2\sum_{i=1}^{m-1}\sum_{l=1}^{o-1}g_2^2(r_i,r_l,t) + v_3\sum_{i=1}^{m-1}\sum_{j=1}^{n-1}g_3^2(r_i,r_j,t)\right],$$

i.e., the energy at T plus the energy lost at the right boundary matches the initial energy plus the energy gained at the left boundary.

4 Convergence of the mimetic numerical scheme

In this section, it is proven that the high-order mimetic discrete analog of the 3D advection equaion flux, when combined with a corresponding high-order time discretization, converges numerically to its classical solution.

To establish convergence of the mimetic numerical scheme, on $V = [-1,1]^3$ and $t \in [0,T]$ with $T = q\Delta t$, one need to show (see [8]) that

$$\lim_{m,n,o,q\to\infty} \|u(x_i,y_j,z_l,t_s) - U(x_i,y_j,z_l,t_s)\| = 0,$$

where

$$x_i = -1 + \left(i - \frac{1}{2}\right)\frac{2}{m}, \qquad y_j = -1 + \left(j - \frac{1}{2}\right)\frac{2}{n}, \qquad z_l = -1 + \left(l - \frac{1}{2}\right)\frac{2}{o}, \qquad t_s = \frac{sT}{q}.$$

However, since the high-order time-discretization LF-MMK utilized for the numerical scheme requires information from several previous time sttage steps, the convergence prove is more involved, since u will be only one component among the other stage variables.

4.1 Mimetic analog of the 3D advection flux term

Equations (1) can be written as

$$u_t = -\nabla\cdot(u\vec{v}). \tag{17}$$

If $\vec{\mathcal{V}} = (V_1, V_2, V_3)$ is the discrete version of the vector field $\vec{v}$, with V_1, V_2, V_3 discrete versions (defined on N) of v_1, v_2, v_3, and U is the discrete version (defined on S) of the scalar field u, then the discrete analog of the right-hand-side of (17) is

$$-D_{xyz}^k(\vec{\mathcal{V}}\circ\mathcal{I}_D^k U) = F_D(U) = K_D U, \tag{18}$$

where $\circ$ is the component-wise product (or Hadamard product), F_D is a discrete linear function of U, and

$$K_D = -\left[D^k_{xyz} \begin{pmatrix} \mathrm{diag}(V_1) & & \\ & \mathrm{diag}(V_2) & \\ & & \mathrm{diag}(V_3) \end{pmatrix} \mathcal{I}^k_D \right].$$

Since $\vec{v}$ is constant and $\nabla \cdot (u\vec{v}) = v_1 u_x + v_2 u_y + v_3 u_z = \vec{v} \cdot \nabla u$, another possible discrete analog of the right-hand-side of (17) is

$$-\mathcal{I}^k_G(\vec{\mathcal{V}} \circ G^k_{xyz} U) = F_G(U) = K_G U, \tag{19}$$

where

$$K_G = -\mathcal{I}^k_G \left[\begin{pmatrix} \mathrm{diag}(V_1) & & \\ & \mathrm{diag}(V_2) & \\ & & \mathrm{diag}(V_3) \end{pmatrix} G^k_{xyz} \right],$$

F_G is a discrete linear function of U, and $\mathcal{I}^k_G$ is the 3D gradient interpolation operator of order $k = 2, 4, 6, 8$ that maps N onto S [6].

By construction, both K_D and K_G are approximations of k-th order of accuracy of $-\nabla \cdot (u\vec{v})$ for constant vector field $\vec{v}$.

4.2 The sixth-order filtered leapfrog scheme

The goal here is to introduce the sixth-order filtered leapfrog scheme LF-MMK [9, p. 2553] and to couple it with the mimetic discretization of the right-hand-sides (18) or (19) of equation (17).

Following [9], consider the ordinary differential equation (ODE)

$$\frac{\partial \psi}{\partial t} = F(\psi), \tag{20}$$

where $F : \mathbb{R}^d \longmapsto \mathbb{R}^d$, for some $d \in \mathbb{Z}^+$.

The formulation of the fifth-order LF-MMK scheme is

$$\psi^{s+1} - \overline{\psi}^{\,s-1} = 2\Delta t \; F(\psi^s), \tag{21}$$

where

$$\overline{\psi}^{\,s-1} = \psi^{s-1} + \gamma_6(\overline{\psi}^{\,s-4} - 5\,\overline{\psi}^{\,s-3} + 10\,\overline{\psi}^{\,s-2} - 10\,\overline{\psi}^{\,s-1} + 5\,\psi^s - \psi^{s+1}). \tag{22}$$

Here, ψ^s is the approximation to the solution at the time $s\Delta t$, and $\overline{\psi}^{\,s}$ is the solution after applying a sixth-order implicit time filter using a real constant γ_6, $0 \leq \gamma_6 \leq 1$, that determines the filter strength.

This linearly implicit scheme is simple enough to be written explicitly [9, p. 2553]. For, if $\overline{\gamma}_6 = (1 + 11\gamma_6)^{-1}$, this scheme can be written as

$$\begin{aligned}
\overline{\psi}^{\,s-1} &= \overline{\gamma}_6(\widetilde{\psi}^{\,s-1} - 2\gamma_6 \Delta t\, F(\psi^s)), && (23)\\
\psi^{s+1} &= \overline{\gamma}_6(\widetilde{\psi}^{\,s-1} + 2(1 + 10\gamma_6)\Delta t\, F(\psi^s)), && (24)\\
\widetilde{\psi}^{\,s} &= \psi^s + \gamma_6(\overline{\psi}^{\,s-3} - 5\,\overline{\psi}^{\,s-2} + 10\,\overline{\psi}^{\,s-1} + 5\,\psi^{s+1}). && (25)
\end{aligned}$$

The time-filtered leapfrog six time levels scheme (21)-(22) requires only four variables to be stored, since (23)-(25) can be seen as an iterative algorithm that overwrites

$$(\overline{\psi}^{\,s-3}, \overline{\psi}^{\,s-2}, \widetilde{\psi}^{s-1}, \psi^s) \qquad \text{by} \qquad (\overline{\psi}^{\,s-2}, \overline{\psi}^{\,s-1}, \widetilde{\psi}^{s}, \psi^{s+1}). \tag{26}$$

In [9, p.2553], it is shown that the amplitude factor of this scheme, when $w\,\Delta t \to 0$, is

$$A_p = 1 - \frac{3\gamma_6}{4}\,\frac{1 + 6\gamma_6}{(1 + 4\gamma_6)^2}\,(w\,\Delta t)^6,$$

and that the phase error of this scheme is (under the same conditions) is

$$R_p = 1 + \frac{1}{6}\,(w\,\Delta t)^2.$$

4.3 The numerical scheme

If one substitutes the linear right-hand-side $F_D(U)$ or $F_G(U)$ into (23)-(25), one obtains the following a high-order mimetic scheme for the 3D advection equation

$$\begin{aligned}
\overline{\psi}^{\,s-1} &= \overline{\gamma}_6(\widetilde{\psi}^{\,s-1} - 2\gamma_6 \Delta t\, K\psi^s), && (27)\\
\psi^{s+1} &= \overline{\gamma}_6(\widetilde{\psi}^{\,s-1} + 2(1 + 10\gamma_6)\Delta t\, K\psi^s), && (28)\\
\widetilde{\psi}^{\,s} &= \psi^s + \gamma_6(\overline{\psi}^{\,s-3} - 5\,\overline{\psi}^{\,s-2} + 10\,\overline{\psi}^{\,s-1} + 5\,\psi^{s+1}). && (29)
\end{aligned}$$

where $K = K_D$ or $K = K_G$, if one uses (18) or (19), respectively.

The iterative process (26) corresponding to (27)-(29) is given by

$$\widehat{\Psi}^{s+1} = M\,\widehat{\Psi}^s, \tag{30}$$

where

$$\widehat{\Psi}^s = (\overline{\psi}^{\,s-3}, \overline{\psi}^{\,s-2}, \widetilde{\psi}^{s-1}, \psi^s)^T \in \mathbb{R}^{4d},$$

and

$$M = \begin{pmatrix}
0 & I & 0 & 0\\
0 & 0 & \overline{\gamma}_6 I & -2\gamma_6\overline{\gamma}_6\Delta t\, K\\
\gamma_6 I & -5\gamma_6 I & 15\gamma_6\overline{\gamma}_6 I & I - 10\gamma_6\overline{\gamma}_6(1 + 12\gamma_6)\Delta t\, K\\
0 & 0 & \overline{\gamma}_6 I & -2\overline{\gamma}_6(1 + 10\gamma_6)\Delta t\, K
\end{pmatrix}, \tag{31}$$

where $\psi^s = U(s\,\Delta t) \in \mathbb{R}^d$ is the actual numerical solution of ODE (20) at time $s\,\Delta t$, and $I = I_{d\times d}$ is the identity matrix with d rows and d columns.

4.3.1 The extended ODE system

System (31) is in terms of $\widehat{\Psi}$ which contains other variables besides the discrete version of ψ. To deal with local truncation errors and global errors for $\widehat{\Psi}$ one needs to extend (20) from the discrete version of ψ to $\widehat{\Psi}$.

The algorithm defined by (23)-(25) converges for certain values of γ_6 and for small Δt [9]. If Δt is small enough then (27)-(28) can be approximated by

$$\begin{aligned} \overline{\psi}^{\,s-1} &\approx \overline{\gamma}_6\, \widetilde{\psi}^{\,s-1} \\ \psi^{s+1} &\approx \overline{\gamma}_6\, \widetilde{\psi}^{\,s-1} \end{aligned}$$

since matrices K are bounded (see Appendix A). Hence, since $\overline{\psi}^{\,s-1} \approx \psi^{s+1}$ then

$$\widetilde{\psi}^{\,s} \approx \psi^s + 11\gamma_6\psi^{s+1} \approx (1 + 11\gamma_6) = (\overline{\gamma}_6)^{-1}\, \psi^{s+1},$$

because for large s, one has $\overline{\psi}^{\,s-3} \approx \overline{\psi}^{\,s-2} \approx \overline{\psi}^{\,s-1}$, and $\psi^{s+1} \approx \psi^s$.

Therefore,

$$(\overline{\psi}^{\,s-2}, \overline{\psi}^{\,s-1}, \widetilde{\psi}^s, \psi^{s+1}) \rightarrow_{s\rightarrow\infty} (\psi, \psi, (\overline{\gamma}_6)^{-1}\, \psi, \psi).$$

It follow that the iterative scheme (27)-(29) can be utilized to find a numerical approximation of the $4d$ constant linear ODE system for $\Psi = (\psi, \psi, (\overline{\gamma}_6)^{-1}\, \psi, \psi)^T$

$$\Psi' = \mathcal{M}\Psi = \begin{pmatrix} K & & & \\ & K & & \\ & & (\overline{\gamma}_6)^{-1}\, K & \\ & & & K \end{pmatrix} \Psi, \tag{32}$$

which has an explicit formula in terms of the eigenvalues and eigenvectors of K (Jordan decomposition).

The Lax-Ritchmyer equivalence theorem [10] implies that one just needs to prove consistency and stability of the scheme (30). Following [8] one can attain both.

For, suppose (32) has a solution Ψ, it holds

$$\Psi(x_i, y_j, z_l, t_{s+1}) = M\, \widehat{\Psi}(x_i, y_j, z_l, t_s) + \Delta t\, \tau^s_{i,j,l},$$

where the local truncation error $\Delta t\, \tau^s_{i,j,l}$ is the difference between the exact solution Ψ and the numerical solution $\widehat{\Psi}$ evaluated at (x_i, y_j, z_l, t_s).

Defining the local error

$$\epsilon^s_{ijl} = \Psi(x_i, y_j, z_l, t_{s+1}) - M\, \widehat{\Psi}(x_i, y_j, z_l, t_s),$$

one gets $\epsilon^0_{ijl} = \Psi(x_i, y_j, z_l, 0) - \widehat{\Psi}(x_i, y_j, z_l, 0)$ as the error on the initial conditions.

Therefore,

$$\epsilon^1_{ijl} = M\,\epsilon^0_{ijl} + \Delta t\,\tau^0_{ijl}.$$

and

$$\epsilon^s_{ijl} = M\,\epsilon^0_{ijl} + \Delta t \sum_{g=0}^{s-1} M^{s-g-1}\tau^g_{ijl}.$$

Considering the global error, one gets

$$\|\epsilon^s\|_{h,p} \leq \|M^s\|_{h,p}\,\|\epsilon^0\|_{h,p} + s\,\Delta t \max_{0\leq g\leq s-1}\{\|M^{s-g-1}\|_{h,p}\,\|\tau^g\|_{h,p}\},$$

where

$$\|A\|_{h,p} = \sup_{w^s_{ijl}} \frac{\|Aw^s_{ijl}\|_{h,p}}{\|w^s_{ijl}\|_{h,p}}, \qquad \|w\|_{h,p} = \left(h\sum_r w^p(r)\right)^{1/p}.$$

The scheme is consistent if

$$\lim_{m,n,o,q} \left\{ \begin{array}{l} \|\epsilon^0\|_{h,p} \\ \max_{0\leq g\leq s-1}\{\|\tau^g\|_{h,p}\} \end{array} \right. = 0. \tag{33}$$

The scheme is stable if

$$\|M^s\|_{h,p} \leq C,$$

for a sufficiently small Δt.

4.3.2 Consistency

If one uses initial data for $\widehat{\Psi}$ that is close to $(u_0, u_0, (\overline{\gamma}_6)^{-1}u_0, u_0)$ and mimetic operators of order four (for the spatial derivatives) and the leapfrog method and sixth-order time filter LF-MMK, then $\|\tau\|_{h,p} = \mathcal{O}(h^4, \Delta t^2)$. For, [1, 2, 3] demonstrate that the order of accuracy of the mimetic scheme is four. Appendix B, exhibits a numerical example that shows that the sixth-order filtered leapfrog scheme LF-MMK is order two accurate.

Hence, (33) holds. So the scheme is consistent.

4.3.3 Stability

It is enough to find an upper bound for $\|M\|_{h,p}$.

Recall that if A is a matrix with m rows, n columns then

$$\|A\|_{\max} \leq \|A\|_2 \leq \sqrt{mn}\,\|A\|_{\max}$$

where $\|A\|_{\max}$ is the max-norm given by

$$\|A\|_{\max} = \max_{1\le i\le m, 1\le j\le n} |a_{ij}|.$$

The max-norm of M is

$$\begin{aligned}
\|M\|_{\max} &= \left\| \begin{array}{cccc} 0 & I & 0 & 0 \\ 0 & 0 & \overline{\gamma}_6 I & -2\gamma_6\overline{\gamma}_6\Delta t\, K \\ \gamma_6 I & -5\gamma_6 I & 15\gamma_6\overline{\gamma}_6 I & I - 10\gamma_6\overline{\gamma}_6(1+12\gamma_6)\Delta t\, K \\ 0 & 0 & \overline{\gamma}_6 I & -2\overline{\gamma}_6(1+10\gamma_6)\Delta t\, K \end{array} \right\|_{\max} \\
&\le \max\{M_0, 2\overline{\gamma}_6(1+10\gamma_6)\Delta t\,\|K\|_{\max}, \|I - 10\gamma_6\overline{\gamma}_6(1+12\gamma_6)\Delta t\, K\|_{\max}\} \\
&\le \max\{M_0, 2\Delta t\,\|K\|_{\max}, 1 + 10\gamma_6\overline{\gamma}_6(1+12\gamma_6)\Delta t\,\|K\|_{\max}\}
\end{aligned}$$

where

$$M_0 = \max\{1, 5\gamma_6, \overline{\gamma}_6, 15\gamma_6\overline{\gamma}_6\}.$$

For the simulations one has $\gamma_6 \approx 0.1$. Hence $M_0 = 1$ and

$$\|M\|_{\max} \le \max\{1, 2\Delta t\,\|K\|_{\max}\}. \tag{34}$$

From Appendix A,

$$\begin{aligned}
K_D &= [v_1\,\mathrm{diag}\{0, I_o, 0\} \otimes \mathrm{diag}\{0, I_n, 0\} \otimes D_x^{(k)} I_{D_x}^{(k)}, \\
&\quad v_2\,\mathrm{diag}\{0, I_o, 0\} \otimes D_y^{(k)} I_{D_y}^{(k)} \otimes \mathrm{diag}\{0, I_m, 0\}, \\
&\quad v_3\, D_z^{(k)} I_{D_z}^{(k)} \otimes \mathrm{diag}\{0, I_n, 0\} \otimes \mathrm{diag}\{0, I_m, 0\}].
\end{aligned}$$

To simplify, assume $m = n = o = \max\{m, n, o\}$.

Since DI_D does not has zero eigenvalues (see Appendix A), it is non-singular and

$$\begin{aligned}
\|K_D\|_{\max} &\le \max\{|v_1|, |v_2|, |v_3|\}\,\|DI_D\|_{\max} \\
&\le \|(v_1, v_2, v_3)\|_1\, \max|\lambda(DI_D)| \le 2\,\|(v_1, v_2, v_3)\|_1.
\end{aligned}$$

The last inequality holds because the spectral radius $\rho(DI_D) < 2$ (see Appendix A).

Therefore, (34) implies

$$\|M\|_{\max} \le \max\{1, 4\,\Delta t\,\|(v_1, v_2, v_3)\|_1\} \le 1 + \alpha\,\Delta t, \tag{35}$$

for $\alpha = 4\,\|(v_1, v_2, v_3)\|$.

Inequality (35) is a sufficient condition for stability (see [8]), since

$$\|M^s\|_{\max} \le \|M\|_{\max}^s \le (1 + \alpha\,\Delta t)^s \le e^{\alpha\, s\,\Delta t} = e^{\alpha\, t_s}.$$

A similar upper bound can be found for $\|K_G\|_{\max}$.

4.3.4 Convergence

Under consistency and stability it follows that the global error holds

$$\|\epsilon^s\|_{h,p} \leq C(t_s) \max_{1\leq g\leq s-1}\{\|\tau^g\|_{h,p}\},$$

where $t_s = s\,\Delta t$, which implies convergence.

Equivalence of discrete norms in $\mathbb{R}^d$ implies that for the mimetic numerical scheme one obtains

$$\|\epsilon^s\|_{h,2} \leq L_1\|\epsilon^s\|_{\max} \leq L_1\|M^s\|_{\max} \max_{0\leq g\leq s-1}\{\|\tau^g\|_{\max}\} \leq L_1 L_2\, e^{\alpha t_s} \max_{0\leq g\leq s-1}\{\|\tau^g\|_{h,2}\},$$

for fixed d and some L_1, L_2. Therefore the mimetic scheme is convergent.

5 Advection example

Consider the following advection equation taken from [9, p. 2546].

$$\frac{\partial\psi}{\partial t} + U\,\frac{\partial\psi}{\partial x} = 0, \tag{36}$$

$U = 10\,ms^{-1}$ in a periodic domain, $\psi_0(x) = \cos(\frac{2\pi x}{l})\,\exp(-\frac{x^2}{d^2})$, where $d = 4\,km$ and $l = 2.5\,km$. (36) is numerically integrated within the domain $-8 \leq x \leq 8\,km$ using a grid spacing of $\Delta x = 100\,m$ and three choices of time steps Δt such hat the corresponding to Courant numbers $\mu = \frac{U\Delta t}{\Delta x}$ are $0.2, 0.4$ and 0.6. Spatial derivatives are approximated by fourth-order Corbino-Castillo mimetic method, and the total number of time steps is chosen so that the initial perturbation is transported one revolution around the domain. The fifth-order filtered leapfrog (LF-MMK) uses $\gamma_6 = 0.1$.

In addition, the fifth-order LF-MMK needs initial data to be able to start. This initial data is obtained by performing a half-step forward Euler followed by three leapfrog steps.

In Figure 1 one can see the evolution and the level of accuracy of the numerical solution of the fifth-order LF-MMK time scheme together with the fourth-order Corbino-Castillo mimetic difference at $400s, 800s, 1200s, 1600s$, respectively.

In addition, the total energy of the solution of the advection equation utilizng the fifth-order LF-MMK time scheme together with the fourth-order Corbino-Castillo mimetic difference at each time step is exhibited in Figure 2. Observe it is almost constant. Only the first steps (which are obtained via a forward Euler and a leapfrog schemes) have a little different total energy.

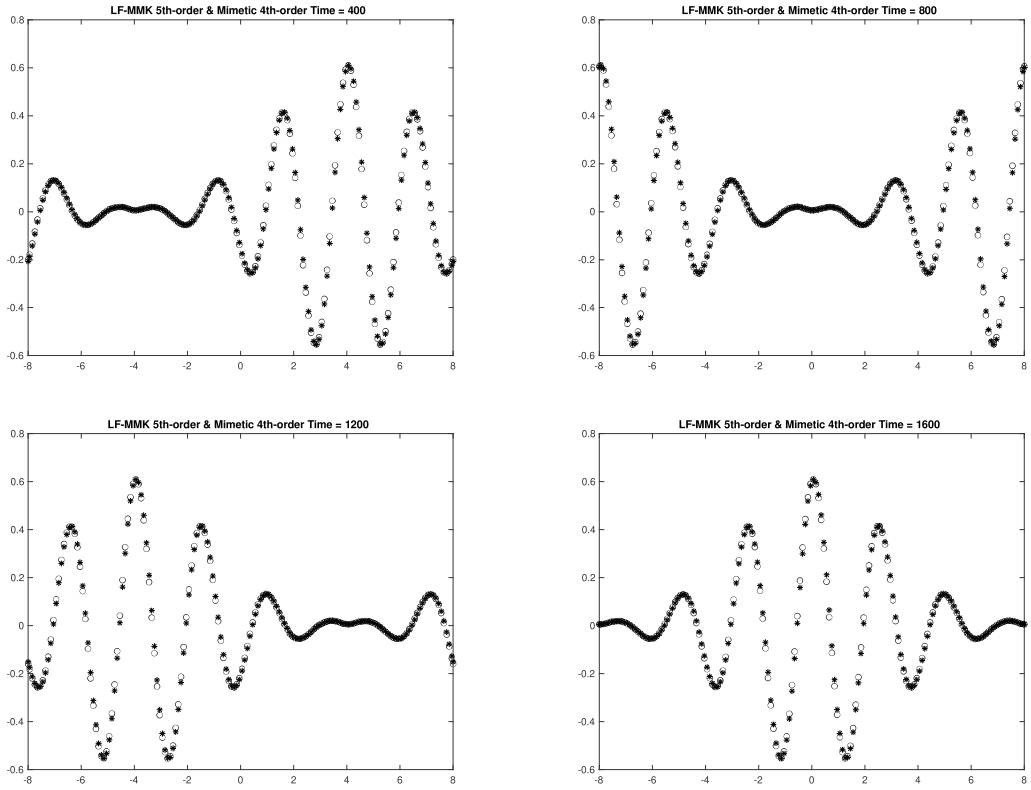

Figure 1: The numerical solution of the 3D advection equation utilizing the fifth-order LF-MMK scheme. The initial condition is displayed on the right lower panel. Some plots of the numerical solution are shown on the left upper (400 s), right upper (800 s), left lower (1200 s), and right lower (1600 s) panels.

6 Conclusions

This paper demonstrates that high-order mimetic discrete analogs of the 3D advection equation conserve theoretically total energy.

In addition, a numerical mimetic scheme of fourth-order in space and the sixth-order filtered leapfrog scheme LF-MMK scheme from [9]) is proposed and a proof of its convergence is given.

Moreover, numerical evidence of conservation of total energy and and numerical convergence are provided.

We plan to explore for higher-order of time discrtization schemes to approximate the so-

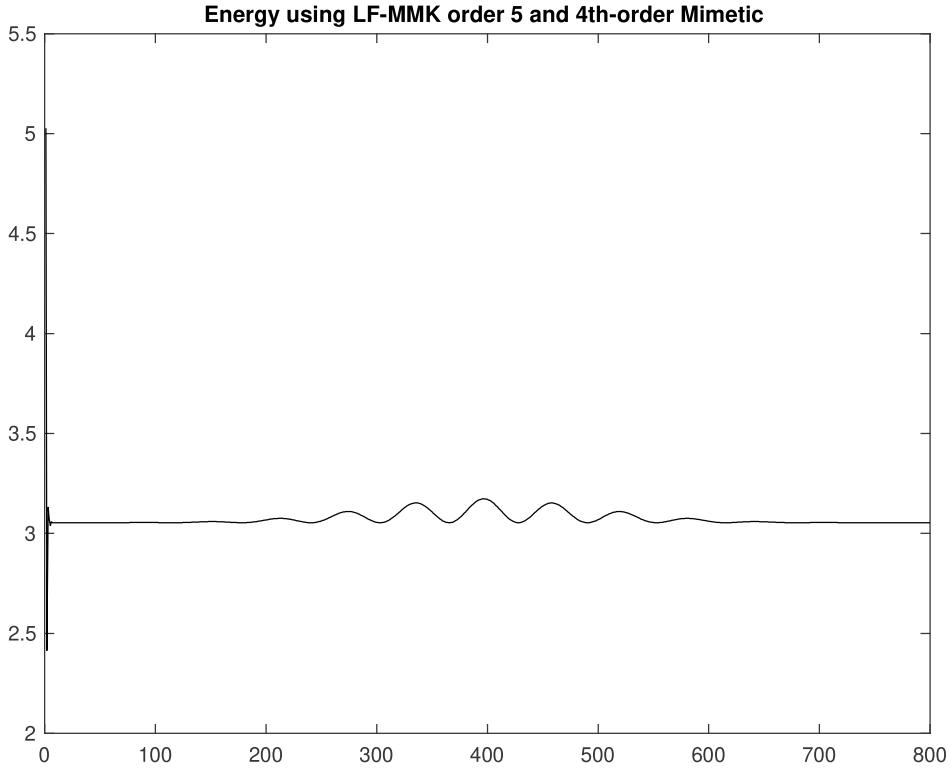

Figure 2: Total energy at each time step of the solution of the advection equation.

lution of the ODE system that develops once a high-order mimetic analog is utilized for discretizing the flux part of the advection equation.

7 Appendix A: Eigenvalues of the mimetic operators

The one-dimensional divergence $D^{(k)}$ mimetic operators of order $k, k = 2, 4, 6, 8$, are represented by non-square matrices, and hence they do not have spectra.

Nevertheless, the divergence, like its continuous analog, applies onto vector fields (whose mimetic data is on the cell edges or staggered grid N) and returns the values of the partial derivatives on the cell interiors S.

However, sometimes the data is on S and to apply the divergence, an interpolation $I_D^{(k)}$ of the data to N is needed before applying the divergence. In [4, p. 1], an exact form to

compute these interpolations operators without the inversion of a Vandermonde matrix is presented.

Therefore, one way of determining the stability of the divergence can be to study the spectra of one-dimensional operator $D^{(k)}I_D^{(k)}, k = 2, 4, 6, 8$.

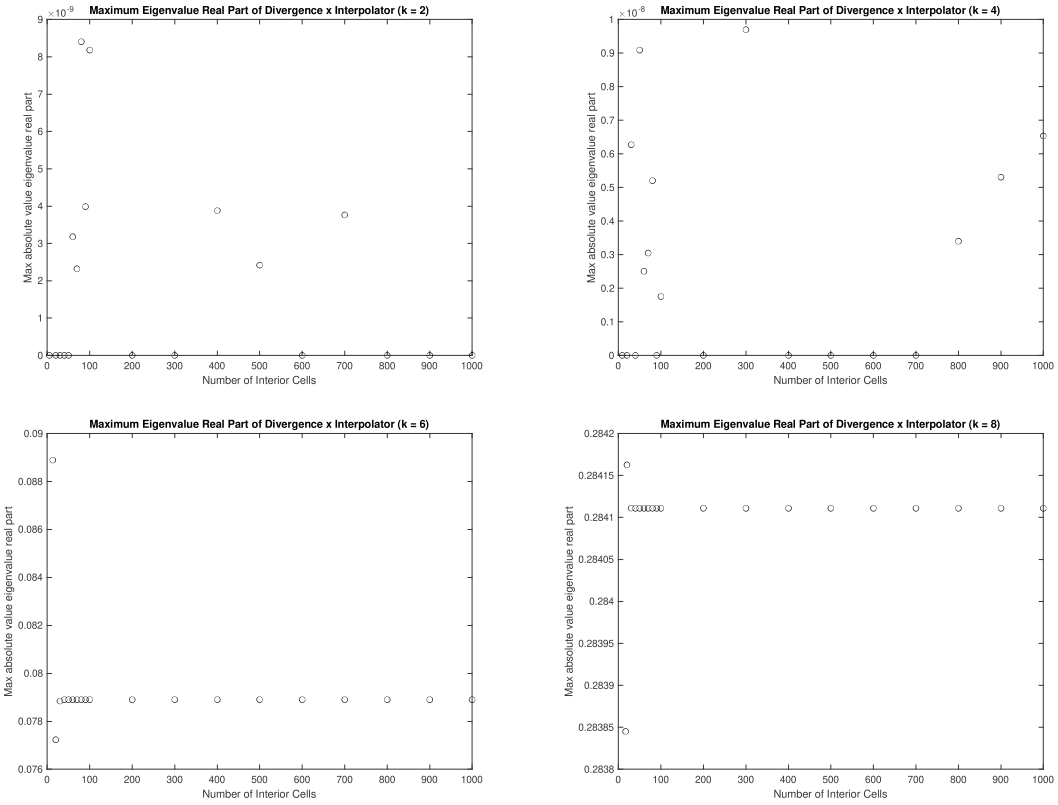

Figure 3: Maximum real part of $D^{(k)}I_D^{(k)}$ eigenvalues in absolute value for $k = 2, 4, 6, 8$, on the top left, top right, bottom left, bottom right panels, respectively.

Figure 3 shows that the maximum real part, in absolute value, of the eigenvalues of the Corbino-Castillo operators $D^{(k)}I_D^{(k)}$, for $k = 2, 4, 6, 8$, are less than 1, for any number of interior cells.

Even though it is not shown, numerically one finds that Corbino-Castillo mimetic operators $D^{(k)}I_D^{(k)}$ eigenvalues for $k = 2, 4, 6, 8$ are not zero.

Figure 4 shows that the maximum module of the eigenvalues of the Corbino-Castillo operators $D^{(k)}I_D^{(k)}$, for $k = 2, 4, 6, 8$, are less than 2, for any number of interior cells.

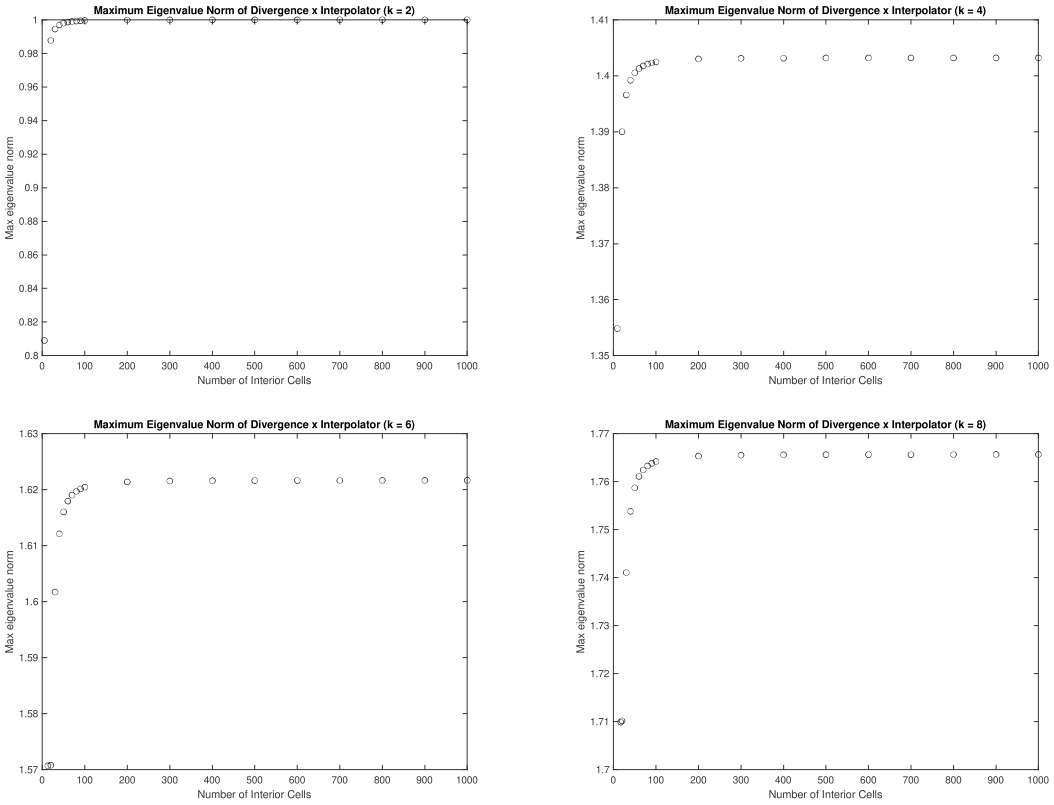

Figure 4: Maximum module of $D^{(k)}I_D^{(k)}$ eigenvalues for $k = 2, 4, 6, 8$, on the top left, top right, bottom left, bottom right panels, respectively.

In the two-dimensional case (with m cells in the x-axis and n cells in the y-axis), the operator $D_{xy}^{(k)}\mathcal{I}_D^{(k)}$ is given by

$$\begin{aligned} D_{xy}^{(k)}\mathcal{I}_D^{(k)} &= [\hat{I}_n \otimes D_x^{(k)}, \quad D_y^{(k)} \otimes \hat{I}_m] \begin{bmatrix} \hat{I}_n^T \otimes I_{D_x}^{(k)} & \\ & I_{D_y}^{(k)} \otimes \hat{I}_m^T \end{bmatrix} \\ &= [\mathrm{diag}\{0, I_n, 0\} \otimes D_x^{(k)} I_{D_x}^{(k)}, \quad D_y^{(k)} I_{D_y}^{(k)} \otimes \mathrm{diag}\{0, I_m, 0\}]. \end{aligned}$$

It is known that for Kronecker products, the eigenvalues $\lambda_{A\otimes B}$ of $A \otimes B$ are obtained by the formula $\lambda_{A\otimes B} = \lambda_A \lambda_B$, where λ_C are the eigenvalues of C.

Therefore, the eigenvalues of $\mathrm{diag}\{0, I_n, 0\} \otimes D_x^{(k)} I_{D_x}^{(k)}$ are given by all possible products of the eigenvalues of $\mathrm{diag}\{0, I_n, 0\}$ (which are two zeros and n ones) and the eigenvalues of $D_x^{(k)} I_{D_x}^{(k)}$, whose maximum real part in absolute value, according to Figure 3, is strictly

bounded above by 1. Hence, the real part of the eigenvalues of $\text{diag}\{0, I_n, 0\} \otimes D_x^{(k)} I_{D_x}^{(k)}$, in absolute value, have 1 as an upper bound.

A similar argument can be applied for the second component of $D_{xy}^{(k)} \mathcal{I}_D^{(k)}$, i.e., $D_y^{(k)} I_{D_y}^{(k)} \otimes \text{diag}\{0, I_m, 0\}$. The real part of its eigenvalues, in absolute value, are also bounded above by 1. Similarly, the norm of its eigenvalues are also bounded above by 2.

An inductive argument demonstrates that the same can be said of the real part of the eigenvalues, in absolute value, of each of the matrix components of the d-dimensional operator $D_{x_1,\cdots,x_d}^{(k)} \mathcal{I}_D^{(k)}$.

A similar process is applicable to the d-dimensional gradient operator.

8 Appendix B: Order of accuracy of the sixth-order filtered leapfrog scheme

The LF-MMK method is utilized to solve the following ODE

$$\psi^{'}(t) = \psi(t), \qquad \psi(0) = 1, \qquad t \in (0, 10).$$

The sixth-order filtered leapfrog scheme uses 1/8-th step of a forward Euler step, followed by three 1/4-th steps to initialize the time discretization scheme.

One can notice in Figure 5 that the order of accuracy of the sixth-order filtered leapfrog scheme LF-MMK is a little above two for the ODE $\Psi^{'} = \Psi$.

References

[1] J.E. Castillo and R.D. Grone, A matrix analysis approach to higher-order approximations for divergence and gradients satisfying a global conservation law, SIAM J. Matrix Anal. Appl., Vol. 25, No. 1, pp. 128-142, 2003.

[2] J.E. Castillo and G.F. Miranda, Mimetic Discretization Method, CRC Press, Boca Raton, Florida, 2013.

[3] J. Corbino, and J.E. Castillo, High-order mimetic finite-difference operators satisfying the extended Gauss divergence theorem, J. Comput. Appl. Math., v. 364, 2020, 112326.

[4] M. Dumett, and J.E. Castillo, Gradient and Divergence Corbino-Castillo Interpolation Operators, CSRC Report, 6-Dec-2022.

[5] M. Dumett, and J.E. Castillo, Energy conservation of second-order mimetic difference schemes for the 1D advection equation, CSRC Report, 7-Dec-2022.

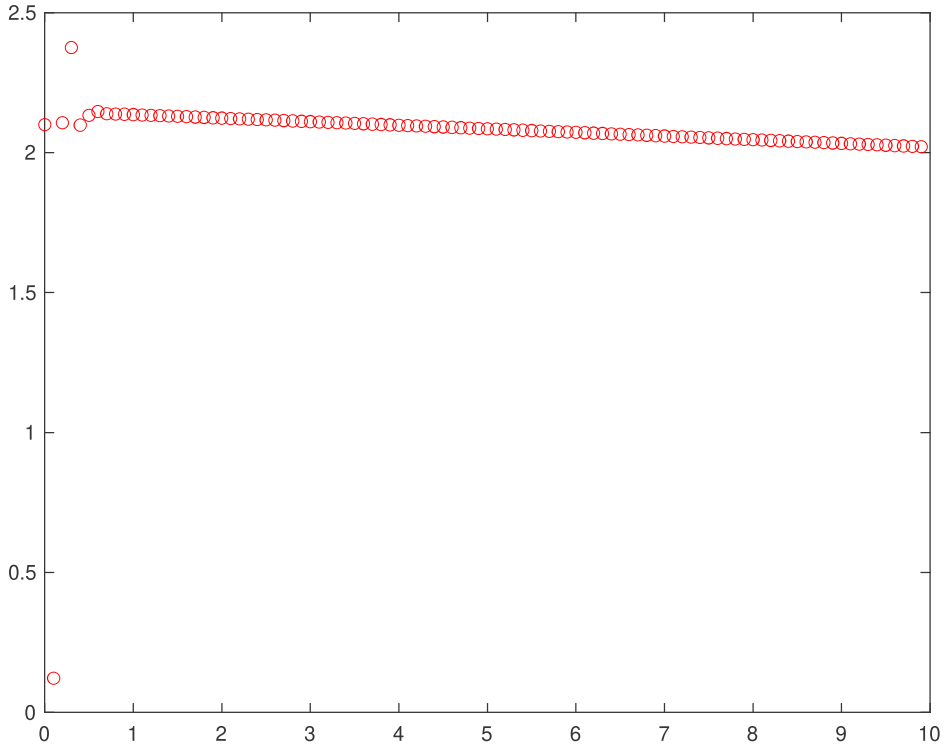

Figure 5: Accuracy order of the sixth-order filtered leapfrog scheme LF-MMK for $\Psi' = \Psi$.

[6] Dumett M.A., and Castillo, J.E., Mimetic analogs of vector calculus identities, San Diego State University, Computational Science Research Center report, CSRCR2023-01, 6-Jul-2023.

[7] L.C. Evans, Partial Differential Equations, Graduate Studies in Mathematics, Vol. 19, American Mathematical Society, Providence, 1998.

[8] J.S. Hesthaven, Numerical methods for conservation laws, SIAM Computational Science and Engineering, Philadelphia, Pennsylvania, 2018.

[9] M. Moustaoui, A. Mahalov, and E.J. Kostelich, A Numerical Method Based on Leapfrog and a Fourth-Order Implicit Time Filter, Mon. Wea. Rev., American Meteorological Society, 2014, Vol. 142, pp. 2545-2560.

[10] J.C. Strikwerda, Finite Difference Schemes and Partial Differential Equations, Second Edition, SIAM, Philadelphia, Pennsylvania, 2004.